CEDTECH International Journal of Engineering & Applied Science
Volume 4, Number 4, December 2023
http://www.cedtechjournals.org
ISSN: 2756-4533

EVALUATION OF W^+ AND W^- BOSON DECAY CHANNEL AT CENTER Of MASS ENERGY IN PROTON-PROTON COLLISION

E.W. Likta, P. B. Teru and N. Ali
Department of Physics,
University of Maiduguri, P.M.B 1069, Maiduguri, Borno State. Nigeria. West Africa.
Email: emmalikta2014@gmail.com

ABSTRACT

It is know that mass-energy is the relationship between mass and energy in a system. The energy E of a particle in its rest frame produce mass with the speed of light and the speed of light is a having a large number in a day unit. Also proton is known as a stable subatomic particle with a positive electric charge. Free protons occur occasionally on Earth like thunderstorms can produce proton with energies of up to several tens of MeV. The goal of this paper is to obtain the differential cross section for different ranges and plotting a graph against fundamental variable. The method used is the computation of Quantum Chromodynamics of cross section. The results obtain is the differential cross section for different ranges. Plotting of graph against fundamental variable has been achieved.

Keywords: *W^+ , W^-, Mass, Energy and Proton*

INTRODUCTION

In physics, mass–energy equivalence is the relationship between mass and energy in a systems rest frame, where the two quantities differ only by a multiplicative constant and the units of measurement (Raymond et al., 2013). The principle is described by the physicist Albert Einstein's formula: (Bodanis, 2009). In a reference frame where the system is moving, its relativistic energy and relativistic mass (instead of rest mass) obey the same formula. The formula defines the energy E of a particle in its rest frame as the product of mass (m) with the speed of light squared (c^2) (Günther et al., 2019). Because the speed of light is a large number in everyday units (approximately 300000 km/s or 186000 mi/s), the formula implies that a small amount of "rest mass", measured when the system is at rest, corresponds to an enormous amount of energy, which is independent of the composition of the matter. Rest mass, also called invariant mass, is a fundamental physical property that is independent of momentum, even at extreme speeds

approaching the speed of light. Its value is the same in all inertial frames of reference. Massless particles such as photons have zero invariant mass, but massless free particles have both momentum and energy. The equivalence principle implies that when energy is lost in chemical reactions, nuclear reactions, and other energy transformations, the system will also lose a corresponding amount of mass. The energy, and mass, can be released to the environment as radiant energy, such as light, or as thermal energy. The principle is fundamental to many fields of physics, including nuclear and particle physics. A proton is a stable subatomic particle, symbol p, H^+, or $^1H^+$ with a positive electric charge of +1 e (elementary charge). Its mass is slightly less than that of a neutron and 1,836 times the mass of an electron (the proton-to-electron mass ratio). Protons and neutrons, each with masses of approximately one atomic mass unit, are jointly referred to as "nucleons" (particles present in atomic nuclei). One or more protons are present in the nucleus of every atom. They provide the attractive electrostatic central force that binds the atomic electrons. The number of protons in the nucleus is defining property of an element, and is referred to as the atomic number (represented by the symbol Z). Since each element has a unique number of protons, each element has its own unique atomic number, which determines the number of atomic electrons and consequently the chemical characteristics of the element.

The word proton is Greek for "first", and this name was given to the hydrogen nucleus by Ernest Rutherford in 1920. In previous years, Rutherford had discovered that the hydrogen nucleus (known to be the lightest nucleus) could be extracted from the nuclei of nitrogen by atomic collisions (Paul et al. 2003). Protons were therefore a candidate to be a fundamental or elementary particle, and hence a building block of nitrogen and all other heavier atomic nuclei. Although protons were originally considered to be elementary particles, in the modern Standard Model of particle physics, protons are now known to be composite particles, containing three valence quarks, and together with neutrons are now classified as hadrons. Protons are composed of two up quarks of charge $+\frac{2}{3}e$ and one down quark of charge $-\frac{1}{3}e$. The rest masses of quarks contribute only about 1% of a proton's mass (Mould et al., 2001). The remainder of a proton's mass is due to quantum chromodynamics binding energy, which includes the kinetic energy of the quarks and the energy of the gluon fields that bind the quarks together (Chow et al.,

2006). Because protons are not fundamental particles, they possess a measurable size; the root mean square charge radius of a proton is about 0.84–0.87 fm (1 fm = 10^{-15}m) (Griffiths et al., 2008). In 2019, two different studies, using different techniques, found this radius to be 0.833 fm, with an uncertainty of ±0.010 fm (Raymond et al., 2013). Free protons occur occasionally on Earth: thunderstorms can produce protons with energies of up to several tens of MeV (Dyson et al., 2019). At sufficiently low temperatures and kinetic energies, free protons will bind to electrons (Stanley et al,. 2003). However, the character of such bound protons does not change, and they remain protons. A fast proton moving through matter will slow by interactions with electrons and nuclei, until it is captured by the electron cloud of an atom. The result is a protonated atom, which is a chemical compound of hydrogen. In a vacuum, when free electrons are present, a sufficiently slow proton may pick up a single free electron, becoming a neutral hydrogen atom, which is chemically a free radical. Such "free hydrogen atoms" tend to react chemically with many other types of atoms at sufficiently low energies. When free hydrogen atoms react with each other, they form neutral hydrogen molecules (H_2), which are the most common molecular component of molecular clouds in interstellar space.Free protons are routinely used for accelerators for proton therapy or various particle physics experiments, with the most powerful example being the Large Hadron Collider.

In particle physics, a boson is a subatomic particle whose spin quantum number has an integer value (0, 1, 2 ...) (Raymond, et al. 2013). Bosons form one of the two fundamental classes of subatomic particle, the other being fermions, which have odd half-integer spin (½, ³⁄₂, ⁵⁄₂,...) (Günther, et al. 2019). Every observed subatomic particle is either a boson or a fermion. Some bosons are elementary particles occupying a special role in particle physics, distinct from the role of fermions (which are sometimes described as the constituents of "ordinary matter"). Certain elementary bosons gluons act as force carriers, which give rise to forces between other particles, while one (the Higgs boson) gives rise to the phenomenon of mass. Other bosons, such as mesons, are composite particles made up of smaller constituents. Outside the realm of particle physics, multiple identical composite bosons (in this context sometimes known as 'bose particles') behave at high densities or low temperatures in a characteristic manner described by Bose–Einstein statistics: for example

a gas of helium-4 atoms becomes a superfluid at temperatures close to absolute zero. Similarly, superconductivity arises because some quasiparticles, such as Cooper pairs, behave in the same way.

MATERIAL AND METHOD

Tree-level contributions with up to two extra patrons, as well as one-loop contributions, were used in the computation of a Quantum Chromodynamics (QCD) cross section at (NNLO)(Laue, 2011). To be correctly appraised, just one patron and entirely virtual donations are needed. In order to apply the scattering amplitude corresponding to these contributions in a complete NNLO calculation, infrared (IR) divergences must be taken into account at the intermediate stage of the calculation. The MATRIX NNLO calculation handles and cancels IR divergence using the qr-subtraction approach, where denotes the transverse momentum of a colorless system (i.e., a system made of particles without QCD interactions) in this formalism(Forshaw, 2009). The cross section for a process pp F+X, where F is a colorless system, may be expressed at NNLO as, in the qr-subtraction technique.

$$do\frac{F}{NNLO} = [do\frac{F+jet}{NLO}\ do\frac{CT}{NNLO}] + H\frac{F}{NNLO}do\frac{F}{O} \qquad 1$$

In equation 1), the cross section for the system F+jet at NLO is represented by the term do (F+jet)/(NLO @), and the cancellation of the F+jet cross section divergence at NNLO is ensured by the process independent counter term do CT/NNLO. The hard-collinear coefficient H F/NNLO at NNLO and the LO cross section do F/O of the system F are combined to complete the computation. Formally, the square-bracketed contribution in equation 1 is finite in the limit QT 0, while the terms do (F+jet)/(NLO @) and do CT/NNLO are independently divergent. A residual dependency parameter with the formula r = qr/m is employed in the NNLO computation using the qr-subtraction technique, where m is the invariant mass of the colorless system. This residual dependency is caused by power-suppressed components, which persist at finite values after the IR singular contribution is subtracted and only disappear at qr 0(Klinkhammer et al., 2014). In order to make both components independently finite, a cut-off number for this residual dependency, rcut, is also introduced. rcut = 0.0015 (0.15%) was utilized in the differential cross section computations of this research at NNLO, and below this cut In order to account for power-suppressed contributions, do (F+jet)/(NLO @) and do CT/NNLO terms were taken to be identical. In

this study, the total cross section is presented for both the extrapolation in the limit of rcut 0 and for rcut = 0.15%.

By including both QCD and electroweak (EW) corrections, the framework's MATRIX also computes for SM processes' NLO precision (Prentis, 2015). The computation of massless and large partons at NLO was carried out using the Catani-Seymour dipole subtraction method. In the Catani-Seymour dipole subtraction technique, a term for subtraction (addition) is incorporated into the computation to cancel each individual divergence of the real and virtual components in their most basic form as follows:

$$\sigma NLO = \int_{m+1} d\sigma_R + \int_{m+1} d\sigma_V = \int_{m+1} [(d\sigma_R)_{\epsilon\to 0} - (d\sigma_A)_{\epsilon\to 0}] + \int_m \left[(d\sigma_R)_{\epsilon\to 0} + \int_1 (d\sigma_A)\right]_{\epsilon\to 0} \quad (2)$$

When integrated for amplitude with m+1 (m) partons in equation (2), dR (dv) stands for the cross section of the real emission contribution (virtual contribution). The words dR and dv are both independently IR divergent(Kragh, 2019). The regularization of the divergences by the subtraction (addition) term dR is integrated across m+1 parton phase-space. The integration of the first term on the right side of equation (2) may be done numerically for the limit pole 0 because the dA term serves as a counterterm for the dR term (Oliphant et al., 2013). Analytically, one parton phase-space leading to the pole may be used to integrate the dR component in the second term on the right side of equation (2). The remaining integration over m parton phase-space may then be carried out numerically after these poles, together with those in dv, cancel any divergences in the limit 0 (Rohlf, 2014).

The LHC's pp collisions with a center-of-mass energy of 13 TeV served as the basis for the cross section estimate of the creation of W + jets in its broadest sense. The MATRIX framework was used to set up the W + jets process in the electron decay channel ppW+ X e+ve+ X, where the W boson is in fact off-shell. To determine how production rates depended on the polarization of the W boson, the W + jets process was divided into W+ X e+ve+ X and W- + X e-v-e + X production (Pound et al., 2010). At most (two) more partons are mentioned in the final stage X of the (N) NLO calculation. Additionally, the cross sections calculations determined that the W boson mass was 80.385 GeV for both the factorization scale F and the renormalization scale R(Laue, 2011). By individually changing the

R and F by a factor of 0.5 and 2, the scales were utilized to estimate uncertainty from missing higher-order contributions in the normal manner. With the exception of situations in which one scale was changed by a factor cross section of 0.5 and the other by a factor of 2 simultaneously, all feasible combinations were employed in the variants (Planck, 2018). In the computations, PDFs from data files were evaluated using the LHAPDF6 (Jammer, 2000). For the computations of the LO, NLO, and NNLO cross sections, respectively, the PDF sets NNPDF30 - to - as - 0118, NNPDF30 - nlo - as - 0118, and NNPDF30 -nnlo-as - 0118 from the NNPDF collaboration were utilized (Frisch et al., 2014). In PDF sets were all based on an EW scale determined by the Z boson mass and a constant strong coupling of s(mz) = 0.18 (John, 2015).

The cross sections were estimated by taking into account actual fiducial cuts on the phase-space that were utilized in LHC experiment data (Le, 2014). In the pseudo rapidity acceptance area of |n|2.4, the lepton (i.e., either an electron or an anti-electron) has to have transverse momentum pT> 25 GeV (Ives, 2012). The anti-KT was used to cluster the jets, and the distance parameter R was set at 0.4. R is defined as R(2+2) considering the separation in both jet n and jet azimuthal angle (Garwin et al., 2012). The criterion for pT> 25 GeV in the velocity acceptance area of |y| 2.4 is a fiducial selection factor for the jets. The jets were chosen for the gluon splitting mechanism gbb, which is crucial for maintaining the safety of jet visible IR. For the electron-neutrino final state neutrinos, pT of the total of all neutrinos (also known as transverse momentum, which is related to the neutrinos' ability to escape detectors in an experiment) had to be more than 20 GeV (Rubakov, 2018). In the end, MT(W) > 0 GeV was utilized, but no fiducial cut was defined for the invariant mass of the W boson, which may be stated using the pT(e), pT-miss, and in the directions of these vectors as,

$$M_T(W) = \sqrt{2}p_T(e)p_T^{miss}(1-\cos\Delta\emptyset) \quad 3$$

While the W boson process-dependent decay channel was previously algorithmically built up in this computation, the MT(W) selection makes sense for experimental observations when a significant background from QCD MultiJet processes must be eliminated (Allain, 2009).

RESULTS AND DISCUSSION

Results

Table 1: Differential cross section as a function for the range from 0-6000

$P_T(W^+)G_eV$	NNLO	NLO	NNLO/NLO
0	125892.5	158489.3	1
50	10000	6309.57	1.5
100	1584.89	1000	1.3
150	251.19	158.49	1.3
200	199.53	102.33	1.25
250	125.89	39.82	1.65
300	15.85	12.59	1.1
350	10	10	1.25
400	7.94	7.94	0.9
450	5.13	5.37	1.5
500	1.99	1.99	2
550	1.58	1.58	1.3
600	1.56	1.26	1.1

Table 2: differential cross section as function for range from 0- 250 G_eV

$P_T(e^+)G_eV$	NNLO	NLO	NNLO/NLO
0	79432.83	79432.82	1.2
15	141253.8	141253.8	1
30	100000	100000	1.3
50	12589.25	11220.18	1.4
65	6309.57	3981.07	1.5
80	1584.89	1412.54	1.3
100	1258.93	1122.02	1.4
115	1000	630.96	1.4
130	630.96	158.49	1.6
150	100	63.19	1.2
165	79.43	50.12	1.7
180	25.12	19.95	1.4
200	17.78	15.85	1.3
215	19.95	14.13	1.8

215	15.85	12.02	2.2
250	14.13	11.22	1.4

Table 3 Differential cross sectionas function for the range 0-600 GeV

	$p_T(j_I)G_e$	NNLO	NLO	NNLO/NLO
1	0	12589.25	11220.18	1
2	50	2511.89	1258.93	1.5
3	100	1258.93	794.33	1.6
4	150	630.96	398.11	1.4
5	200	251.19	100	2
6	250	100	39.81	1.8
7	300	39.81	12.59	1.8
8	350	25.12	11.22	1.6
9	400	15.85	7.94	5.2
10	450	7.94	5.01	3
11	500	5.01	3.16	4
12	550	3.98	1.99	3
13	600	3.16	1.26	2

Table 4 Differential cross section as function for the range 0-2.4

	$p_T(j_I)G_e$	NNLO	NLO	NNLO/NLO
1	0	208929.6	173780.1	1.5
2	0.2	204173.8	165958.7	1.4
3	0.4	204173.8	165958.7	1.45
4	0.6	199526.2	162181	1.4
5	0.8	190546.1	151356.1	1.45
6	1	181970.1	147910.8	1.44
7	1.2	173780.1	141253.8	1.44
8	1.4	169842.4	134825.3	1.45
9	1.6	165958.7	131825.7	1.35
10	1.8	162181	128825	1.5
11	2	158489.3	125892.5	1.43
12	2.2	151356.1	120226.4	1.55
13	2.4	144544	114815.4	1.55

Table 5 Differential cross section as a function for the range 0-2.4 of (e^+)

$\eta\ (e^+)$	NNLO	NLO	NNLO/NLO
0	1230269	1230268.8	0.96
0.2	1258925	1258925.4	0.98
0.4	1318257	1288249.6	1
0.6	1348963	1318256.7	1.04
0.8	1348963	1318256.7	1.05
1	1348963	1348962.9	1.04
1.2	1318257	1318256.7	1
1.4	2348963	1318256.7	1.07
1.6	1318257	1318256.7	1.04
1.8	1348963	1318256.7	1.1
2	1348963	1348962.9	1.03
2.2	1318257	1318256.7	1
2.4	1318257	1318256.7	1

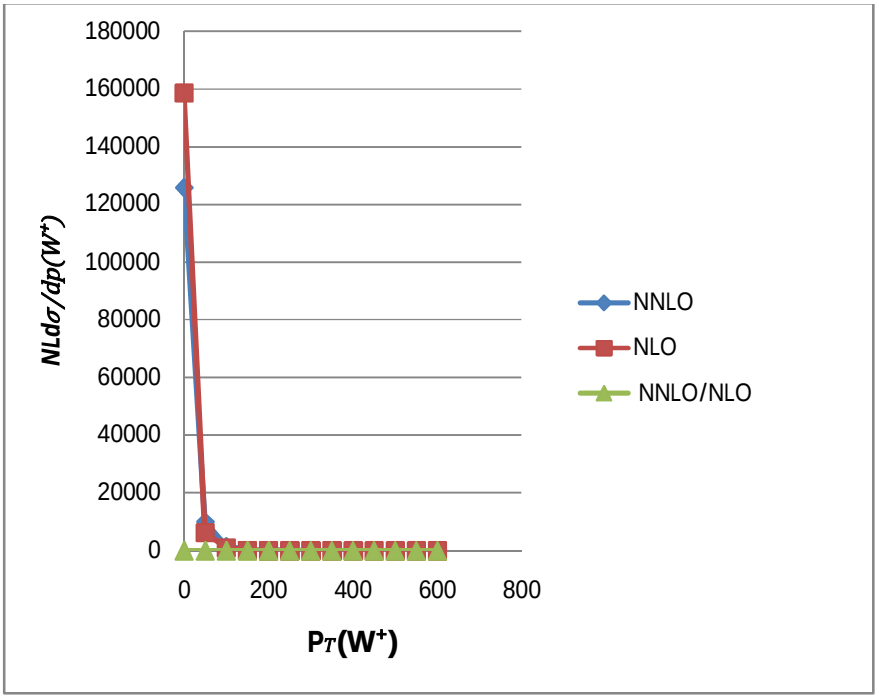

Figure 1:$P_T(W^+)$ against NL $d\sigma/dp\ (W^+)$ for differential cross section of the range from 0-6000
Where NNLO/NLO to be NL

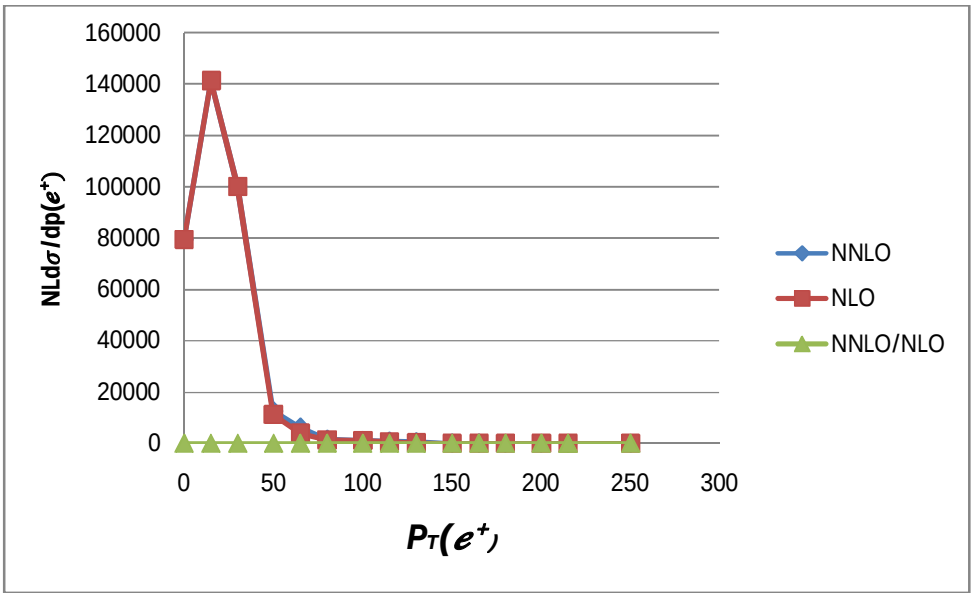

Figure 2: P_T (e^+) against NL dσ/dp (e^+) for differential cross section of range from 0- 250 G_eV

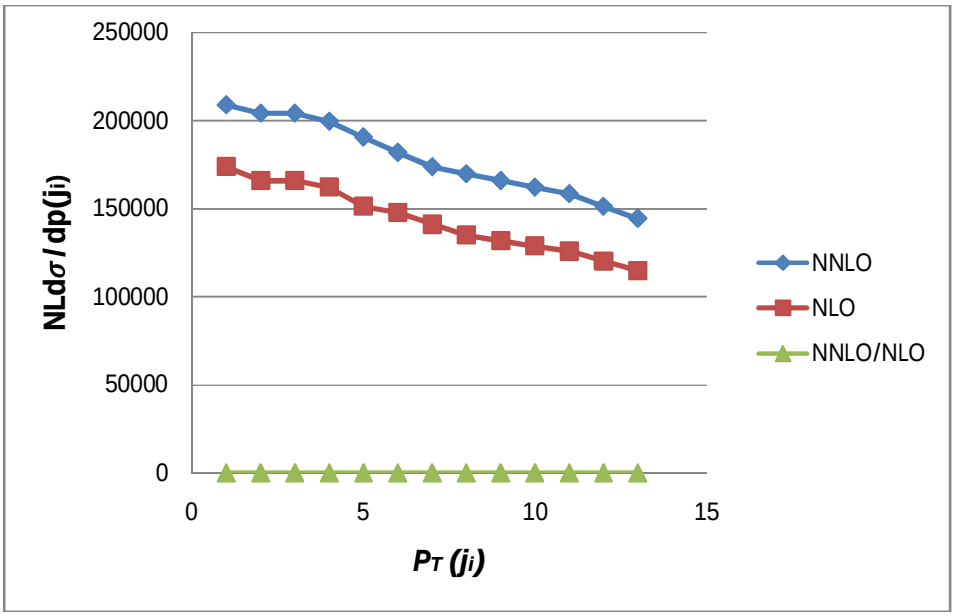

Figure 3: P_T (j_i) against NL dσ/dp (j_i) for differential cross section of the range 0-600 G_eV

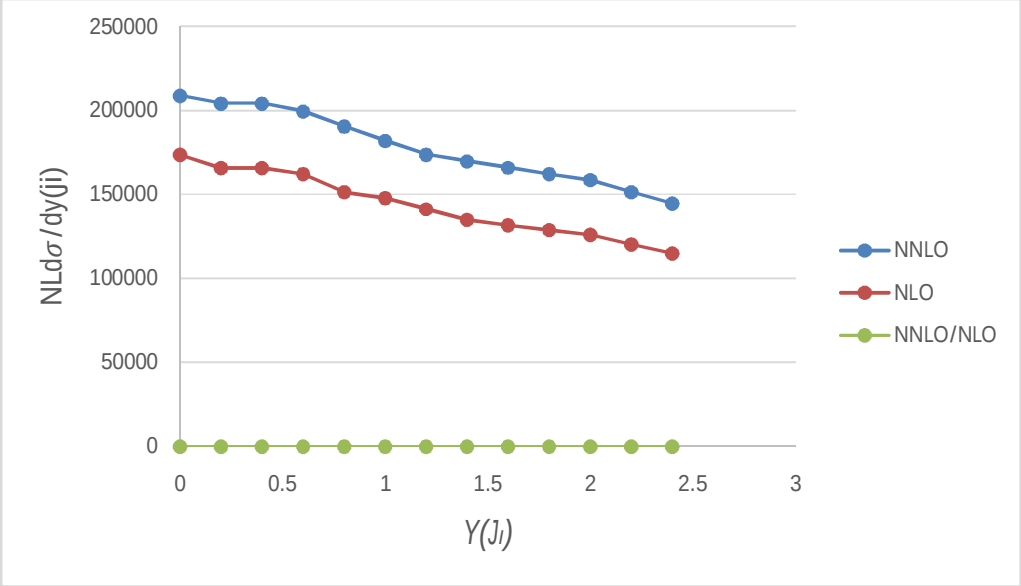

Figure 4:Y(j_i) against NL dσ/dp (j_i) of differential cross section of the range 0-2.4 GeV.

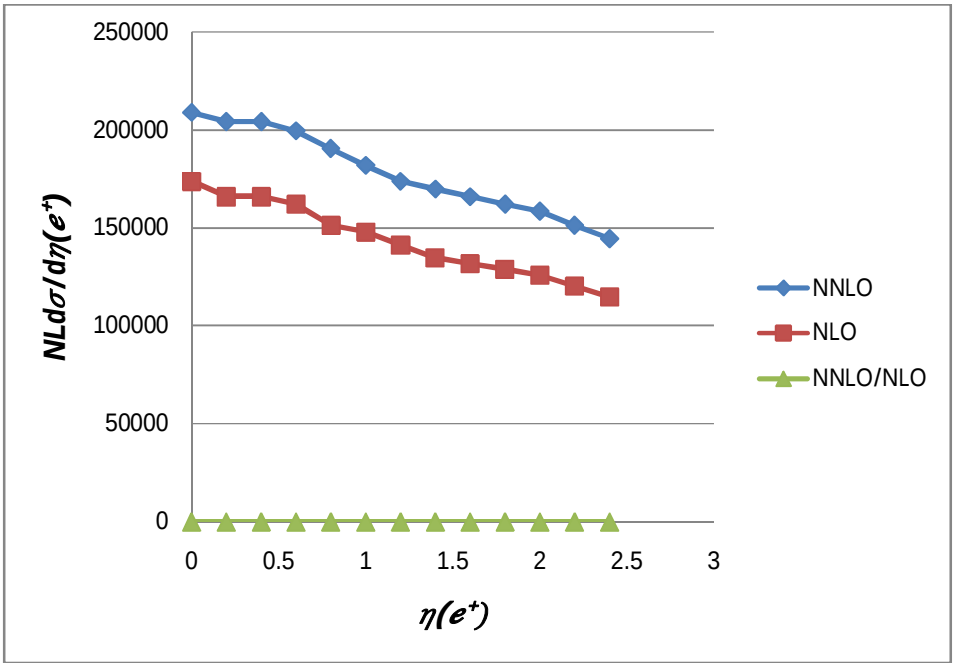

Figure 5:(e^+) against NL dσ/dp(e^+) of differential cross section of the range 0-2.4

DISCUSSION

The jet multiplicity Njet in the fiducial phase-space was used to compute the differential production cross sections for the W+ jets process. In Tables 1 and 2, the differential cross sections were estimated for up to one jet at NLO and up to two jets at NNLO, respectively. Table 3 lists the varied outcomes for the MT (W) variable of the W boson in each area. The % to the center results also includes the maximum and minimum scale uncertainty. Comparing the differential cross sections measured at NLO and NNLO, the W+ boson decay channel has greater cross sections than the W- boson decay channel. At NNLO, the differential cross sections' uncertainties were greatly decreased. For differential cross sections at NNLO, the uncertainties were down to or below the 2% threshold. A specific range determines how the uncertainties for MT (W) are compared, although overall, the precision of the NNLO differential findings above those of the NLO is higher. Table 1 shows the differential cross section for the W+ + X e+ ve + X and W- + X e- ve + X processes, estimated up to one jet at NLO, as a function of Njets. The scale uncertainties caused by changes in R and F are expressed as percentages. For the W++ X e+ve+ X and W-+ X e-ve-+ X processes, the differential cross sections as a function of Njets were estimated up to two jets at NNLO.

The differential cross sections for the W++ X e+ve +X and W-+ X e-ve-+ X processes determined at NNLO, expressed as bins of MT (W). The outcomes are shown for the MT (W) ranges between 0 and 1000 GeV. The fiducial phase-space PT(w), PT(ji) were used to construct the differential cross section distribution for the W+ jets process. In computations of cross sections, the PT is a significant variable that is more sensitive to higher order adjustments. For comparisons, the PT distributions were computed at NLO and NNLO and superimposed in the same figure. Figures 1-3 provide the differential distributions for the PT (w) and PT (ji), respectively. The PT of the first leading jet—the hardest jet according to PT—is displayed in the PT (ji) distributions. Additionally, in order to account for variables employed in the fiducial phase-space definition in addition to the PT variable, the differential distribution cross sections were computed as functions of the leading jet absolute rapidity |y(ji)| and the electron (anti electron) absolute pseudo rapidity |n(e)|. Figures 4 and 5 illustrate how the |y(ji)| and |n(e)|distributions, which were estimated at NLO and NNLO,

respectively, were superimposed in the same plot for comparisons. To more effectively compare NLO and NNLO results in the W+ and W- boson decay channels, the differential distributions for the W+ and W- boson decay channels are included in each plot. In each differential distribution, the core points are surrounded by hatching bands that represent the systematic uncertainty resulting from changes in the R and F scales. While the NNLO computation indicated somewhat greater differential cross sections for the upper ranges of the PT variables, the forms of the distributions were generally consistent at NLO and NNLO for the PT variables. Any peak that is absent from the low-PT (W) area of the differential PT (W) distributions is not considered a non-perturbative impact of soft gluon radiation in these (N) NLO perturbative computations. Different subtraction techniques utilized in the computations may be the cause of the variation in the differential forms for the upper ranges of the PT (ji) variable at NLO and NNLO. Different subtraction techniques that were applied in the calculations may be the cause of the PT (ji) variables NLO and NNLO. The P_T *(e)* differential distribution shapes were almost comparable; however, the P_T*(e)* spectrum was lower than P_T*(ji)* spectrum implying.

The results at different accuracies show that W-boson is less produced than W+ boson in PP collisions. The ratio of the cross sections is $\sigma_{W^-}/\sigma_{W^+}\approx 0.76$, which is essentially independent of the perturbative order of the calculated cross sections. The difference in the production rates points to a strong asymmetry in the electron decay channels of the W boson. In addition to this interpretation, the best cross section at the qt-subtraction formalism. The total rates were predicted to be higher in $\sigma_{NNLO}^{\text{extrapolated}}$ ***results than*** σ_{NNLO}^{rcut}ones implying that QCD corrections at NNLO were better handled using the $r_{cut}\rightarrow 0$ extrapolation approach. This observation is supported by Table 5, where the KNNLO extrapolated values were noticeably greater than the KNNLOrcut values. From LO findings to NLO and NNLO computations, the total cross section results' accuracy was increased. At LO, the scale variation-related uncertainties were at a level of 14%; however, they dropped to -5% at NLO and -1% at NNLO. The total production cross sections for the W+ + X e+ve + X and W- +X e- ve- + X processes estimated at LO, NLO, and NNLO in the fiducial phase-space. The NNLOcross sections are presented for the extrapolation in the limit rcut (NNLO extrappolated) and for the fixed cut-off value rcut the = 0.15% (NNLOrcut).In addition

to the center %, the scale uncertainties caused by differences in R and F are provided in percent. The relative magnitude of the higher order corrections in the W+ + X e+ve + X and W- +X e- ve + X and NNLO decay channels' W+ + X e+ve + X and NNLO cross sections.

CONCLUSION

The fiducial phase-pace of the W boson generation in connection with jets in pp collisions at center of mass energies of the differential cross sections and the overall cross sections. At the perturbative orders of NLO and NNLO, the cross sections for the W+ + X e+ve + X and W- +X e- ve- + X decay modes were determined. Realistic fiducial cuts were employed in computations using the MATRIX computing framework for the W boson decay products. In order to calculate the NLO, the catani-Seymour dipole subtraction technique was employed. On the other hand, the IR divergences in the NNLO computation were evaluated using the qr-subtraction approach. Using the qr-subtraction approach, the NNLO differential cross sections were calculated using a fixed residual dependency parameter cut rcut = 0.15%. The computation of the total production cross sections at NNLO contained systematic errors resulting from changes in the R and F scales, which are taken into account when estimating the perturbative uncertainties at each order. The cross sections calculations that are based on a constant strong coupling of s (ms) = 0.118 employ the NNPDF30 PDF set. Finally, calculated differential and total cross sections may be utilized to compare to experimental results. Specifically, the NNLO differential computations using the qT-subtraction method. In terms of precision, the NNLO differential calculations conducted in the fiducial phase-space of W+jets generation are already satisfactory.

REFERENCE

Allain R.(2009): Rotational Energy of the Earth as an energy source. Wired, pp1028 -1059.

Bodanis, D. (2009). $E=mc^{12!}$: A Biography of the World's Most Famous Equation

Chow T. L. (2006). Introduction to Electromagnetic Theory: A Modern Perspective. Jones & Bartlett Learning p. 392.

Dyson, F.W., Eddington, A.S. and Davidson, C.R. (2019): A determination of the deflection of light by the sun's gravitational

field, from observations made at the total eclipse. Philosophical Transactions of the Royal Society of London. Series A, Containing Papers of a Mathematical or Physical Character. **220** (571–581): 291–333.

Forshaw J. R. (2009). Dynamics and relativity. Smith, A. Gavin. Chichester, UK: John Wiley & Sons. p. 259.

Frisch D. H and Thorndike A. M (2014). Elementary particles. Princeton, N.J.: D. Van Nostrand. pp. 11–12.

Garwin R. L. and Charpak G. (2012). Megawatts and Megatons: The Future of Nuclear Power and Nuclear Weapons (illustrated ed.). University of Chicago Press.p. 17.

Griffiths D. J. (2008). Introduction to elementary particles (2nd, rev. ed.). Weinheim (Germany): Wiley-VCH. p. 101

Günther, H. and Müller V. (2019), Special Theory of Relativity: Einstein's World in New Axiomatics Einstein's Energy–Mass Equivalence, Singapore: Springer, pp. 97–105,

Ives H. E. (2012): Derivation of the Mass-Energy Relation. Journal of the Optical Society of America. **42** (8): 540.

Jammer M. (2000). Concepts of mass in contemporary physics and philosophy. Princeton, N.J.: Princeton University Press. p. 51.

John M. (2015):The Yields of the Hiroshima and Nagasaki Nuclear Explosions. Los Alamos National Laboratories.

Klinkhammer, F. and Manton, N. (2014): A Saddle Point Solution in the Weinberg Salam Theory. Physical Review D. **30** (10): 2212.

Kragh H. (2019): Fin-de-Siècle Physics: A World Picture in Flux. Quantum generations: a history of physics in the twentieth century. Princeton University Press. pp. 3–12.

Laue, M. (2011): ZurDynamik der Relativitätstheorie. On the Dynamics of the Theory of Relativity. Annalen der Physik (in German). **340** (8): 524–542.

Le B. G, (2014): The evolution of forces. The Energetical Explanation of Phenomena. Nuclear Physics B.,Vol. 319, pp570-622.

Mould R. A. (2001). Basic Relativity. Springer Science & Business Media.p. 126.

Oliphant, M. L. E., Kinsey, B. B. and Lord R. (2013). "The Transformation of Lithium by Protons and by Ions of the Heavy Isotope of Hydrogen". Proceedings of the Royal Society. **141** (845): 722–733.

Paul A. T. and Llewellyn R. A. (2003): Modern physics. New York: W.H. Freeman. 4th ed, pp. 87–88.

Planck, M. (2018): ZurDynamikbewegterSysteme. On the Dynamics of Moving Systems. Annalen der Physik (in German). **331** (6): 1–34.

Pound R. V. and Rebka, G. A. (2010): Apparent Weight of Photons. Physical Review Letters. **4** (7): 337–341.

Prentis, J. J. (2015): Why is the energy of motion proportional to the square of the velocity?. American Journal of Physics. **73** (8): 701–707.

Raymond A., Jewett J. W. and Peroomian V. (2013). Physics for scientists and engineers with modern physics. Boston, MA, 9th ed, pp. 1217–1218.

Rohlf J. W. (2014). Modern physics from α to Z^0 (1st ed.). New York: John Wiley. p. 20.

Rubakov, V. A. (2018): Monopole Catalysis of Proton Decay. Reports on Progress in Physics. **51** (2): 189–241.

Stanley M. (2003): 'An Expedition to Heal the Wounds of War. The 1919 Eclipse and Eddington as Quaker Adventurer. Isis. **94** (1): 57–89.